Journal of Marine Systems 158 (2016) 120–128

Contents lists available at ScienceDirect

Journal of Marine Systems

journal homepage: www.elsevier.com/locate/jmarsys

Source waters for the highly productive Patagonian shelf in the southwestern Atlantic

Hajoon Song*, John Marshall, Michael J. Follows, Stephanie Dutkiewicz, Gaël Forget

Department of Earth, Atmospheric and Planetary Sciences, Massachusetts Institute of Technology, Cambridge, United States

ARTICLE INFO

Article history:
Received 3 November 2015
Received in revised form 9 February 2016
Accepted 23 February 2016
Available online 3 March 2016

Keywords:
Patagonian shelf
Nutrient sources
Adjoint sensitivity analysis
Vertical mixing
Southern Ocean

ABSTRACT

Possible nutrient sources and delivery mechanisms for the highly productive Patagonian shelf in the southwest Atlantic are identified. Using a passive tracer adjoint sensitivity experiment, we identify three source waters: waters local to the Patagonian shelf, coastal waters near the Chilean coast and the subsurface waters in the southeast Pacific. We perform a series of forward simulations of a biogeochemical model to investigate the impact of nutrient perturbations in these source regions to productivity on the Patagonian shelf.

Positive nitrate perturbations from local waters have an immediate impact elevating productivity. Iron perturbations local to the shelf, however, do not change productivity because the shelf region is limited by nitrate. Additional nutrient supply from the other source regions leads to increases in productivity. We find that positive nutrient perturbations in subsurface waters in the southeast Pacific result in the largest boost of productivity over the shelf. These source waters are rich in nutrients and upwelled from the depth where light levels are so low that they cannot be consumed. Finally, we identify wintertime intense vertical mixing as the key process which draws nutrients from below 300–500 m to the surface before being delivered to the shelf.

1. Introduction

The South Atlantic ocean to the east of Patagonia is one of the most biologically productive regions in the global ocean (Acha et al., 2004; Bisbal, 1995; Palma et al., 2008) resulting in a very rich and diverse community (Romero et al., 2006). The high productivity can be clearly seen in observations of chlorophyll-a from space with the maximum near the shelf-break (Machado et al., 2013; Rivas et al., 2006; Romero et al., 2006).

The Patagonian shelf region is a significant sink of atmospheric carbon dioxide (CO_2). Padín et al. (2010) suggested the Patagonian shelf as the strongest CO_2 uptake region in the Atlantic based on a survey between Spain and the Southern Ocean. It is likely one of the most intense sinks per unit area in the global ocean (Bianchi et al., 2005, 2009), with annual uptake rates rivaling those in the subpolar North Atlantic. In particular, the southwest Atlantic appears to be an area where the biological forcing of the CO_2 air–sea exchange exceeds that of solubility (Takahashi et al., 2002), implying that vigorous biological activity is largely responsible for net annual uptake of CO_2.

High community productivity requires sufficient supply of both macronutrient (e.g. nitrate, nitrite, phosphate and silica) and micronutrient (e.g. iron). Hence, the distribution of the nutrients, their sources and delivery mechanisms are of great interest. Sabatini et al. (2004) explore the zooplankton hotspot in the Grande Bay on the southern Patagonian shelf, and suggest that elevated nutrient levels originate from land, river and runoff from the Magellan and Fuegian Channels, as well as frontal upwelling.

Acha et al. (2004), on the other hand, argue that high levels of chlorophyll biomass found near the shelf break area are associated with nutrient supply by the Malvinas Current. Nutrient-rich subantarctic water flows northward and provides nutrients to the shelf area through various physical processes including eddies and mixing. Romero et al. (2006) also identify the Malvinas Current as a nutrient source supporting high levels of chlorophyll near the shelf break. Additionally, convergence in the bottom boundary layer and subsequent upwelling can supply nutrients to the Patagonian shelf break.

Garcia et al. (2008) analyze sampled nutrients from a cruise in November 2004 along and across the shelf break fronts and argue that macronutrient is supplied from the Malvinas Current through upwelling along the front. They also suggest four mechanisms of iron supply: frontal upwelling delivering subsurface iron in the Malvinas Current to the euphotic zone, tidal mixing that lifts iron in sediment in the shallow shelf area, deposition of dust and influence of iron-rich groundwater from remote regions.

* Corresponding author. Tel.: +1 617 253 0098.
E-mail address: hajsong@mit.edu (H. Song).

http://dx.doi.org/10.1016/j.jmarsys.2016.02.009
0924-7963/

Using the data collected from a series cruises along the Patagonian shelf during 2001 and 2003, Paparazzo et al. (2010) show that nitrate is nearly depleted and negatively correlated with chlorophyll in summer, indicating that nitrate is the limiting nutrient on the Patagonian shelf. They further identify the decreasing trend of nitrate moving toward the equator along the shelf, which perhaps hints at the source of nitrate. Subantarctic waters with a high level of nitrate penetrate onto the shelf through the gap between Tierra del Fuego and the Malvinas Islands and travel equatorward along the shelf. One might then expect nitrate levels to naturally decrease as it is consumed and mixed with surrounding water masses.

These studies reveal the importance of nitrate and iron sources contributing to high productivity over the Patagonian shelf and suggest controlling physical mechanisms on a regional scale. However, it is still unclear how the supply of nutrients is linked to the large-scale ocean circulation, particularly upstream of Drake Passage.

In this study, we seek to understand the sources of nutrients and the physical processes of delivery from a large-scale perspective. To explore the origin of the source water we conduct an adjoint model with a passive tracer. The adjoint tracer approach is a powerful tool to identify water sources for a chosen area (see Chhak and Di Lorenzo, 2007; Fukumori et al.,2004; Song et al., 2011). In addition, it underscores the processes responsible for the delivery since it integrates backward in time. Results from the adjoint model simulation are evaluated using a series of forward biogeochemical model simulations with perturbations to the nutrients in the source water regions. The results indicate that vertical mixing is the key process bringing nutrient-rich water to the surface.

Our paper is organized as follows. The description of the adjoint model using a passive tracer and the forward biogeochemical model with nutrient perturbations is given in Section 2. Results from these numerical experiments are presented in Section 3. Section 4 discusses nutrient supply to the region of interest, the spatial patterns of response in productivity and the possible connection between the observed increasing trend of chlorophyll biomass and nutrient supply. We conclude in Section 5.

2. Experimental design

The numerical experiments are carried out using the Massachusetts Institute of Technology General Circulation Model (MITgcm) (Adcroft et al., 1997; Adcroft and Marshall,1999; Marshall et al., 1997a,b, 1998). The global ocean model is configured following Estimating the Circulation and Climate of the Ocean (ECCO version 4) (Forget et al. (2015a), available at http://mit.ecco-group.org/opendap/ecco_for_las/version_4/release1/contents.html). The parameter values for the turbulent transport of geostrophic eddies (Gent and McWilliams, 1990) and isopycnal diffusion (Redi, 1982) are both 850 $m^2\ s^{-1}$ which is smaller than that in ECCO version 4. The vertical diffusivity for tracers is $1 \times 10^{-5}\ m^2\ s^{-1}$. The ECCO version 4 initial condition is integrated freely for one year with the normal year Common Ocean-ice Reference Experiments version 2 (CORE-II) surface forcing.

A simple biogeochemical model is coupled to the physical system to simulate the transport of 6 biogeochemical tracers including both micro and macro nutrients (Dutkiewicz et al., 2005; Parekh et al., 2006; Verdy et al., 2007). This biogeochemical model includes a representation of the biological uptake of inorganic nutrient (NO_3, Fe) as a function of nutrient limitation and light availability. This biological uptake is termed here "community production" as it includes the impact of both primary producers and herbivores (see Appendix A). This model was integrated for a long period of time (>300 years) along with the global ocean circulation model with the normal year CORE-II surface forcing to get a quasi-equilibrium biogeochemical state for an initial condition.

The adjoint model integrates the sensitivity of a cost function J to model parameters backward in time. It has proven to be a powerful tool in many studies such as heat transport sensitivity (Marotzke et al., 1999), carbon sequestration efficiency (Hill et al., 2004), sensitivity of biological production and air–sea CO_2 exchange (Dutkiewicz et al., 2006), ocean circulation and ecosystem in California Current System (Moore et al., 2009), Pacific sardine spawning habitat (Song et al., 2012) and bottom pressure of the Arctic Ocean (Fukumori et al., 2015).

In our study, we define a cost function J as the total amount of passive tracer at the surface over the Patagonian shelf during the last two weeks of the year when the shelf is biologically productive:

$$J = \int_{T-\Delta t}^{T} \int_{A} C \Delta z dA dt, \tag{1}$$

where T is December 31st, Δt is 2 weeks, A is the size of the area of interest, C is the surface passive tracer concentration which is set to 1, and Δz is the thickness of the model's surface layer. The adjoint model is integrated backward in time for one year to find the source waters of the Patagonian shelf.

We further verify the result from the adjoint experiment with a series of forward integrations of the biogeochemical model. This is prudent because the adjoint model experiment is carried out with passive tracers, and so results do not necessarily apply to biogeochemical variables which experience additional sources and sinks. We therefore perturb nutrient concentrations at the source guided by the adjoint and monitor subsequent changes over the Patagonian shelf.

We assume that the size of perturbation in x_i, the ith element of the state $\mathrm{x} = [x_1,\ x_2,\ \cdots,\ x_N]$, is proportional to its contribution to J so that no perturbation is introduced in the regions which do not provide water to the area of interest. A perturbation δx_i is expressed as

$$\delta x_i = \frac{\partial J / \partial x_i}{\Sigma_{i=1}^{N} (\partial J / \partial x_i)^2} \delta J. \tag{2}$$

We perturb NO_3 or Fe by an amount that would lead to a 10% increase in J over the area of interest in December. If they are delivered without consumption, we expect the NO_3 or Fe levels to increase by 10% at the Patagonian shelf. A lesser increase would suggest a net loss of nutrients along their path. We also monitor the changes in community productivity at the Patagonian shelf and offshore of the shelf break to explore the impact of nutrient perturbations in the water source regions.

After a series of forward experiments in which the initial time was varied, we chose June 1st as the starting date. We also performed additional experiments which started earlier than June, but the responses in the target area were not significantly different. These suggest that the 7-month forward integration begun on June 1st is long enough to capture most of the physical and biological processes associated with the nutrient delivery and the winter preconditioning of biological activity.

3. Results of forward and backward calculations

3.1. Simulated biogeochemical ocean states

The biogeochemical simulation is first evaluated by comparing it with a climatology and with observations (Fig. 1). The zonal mean of simulated NO_3 generally agrees well with the World Ocean Atlas 2009 climatology in the Southern Ocean (Fig. 1 (a, b)), showing an increase toward Antarctica and with depth. The simulated Fe is compared with three meridional sections (Fig. 1 (c–e)). Two meridional sections upstream of Drake Passage show near-depletion at

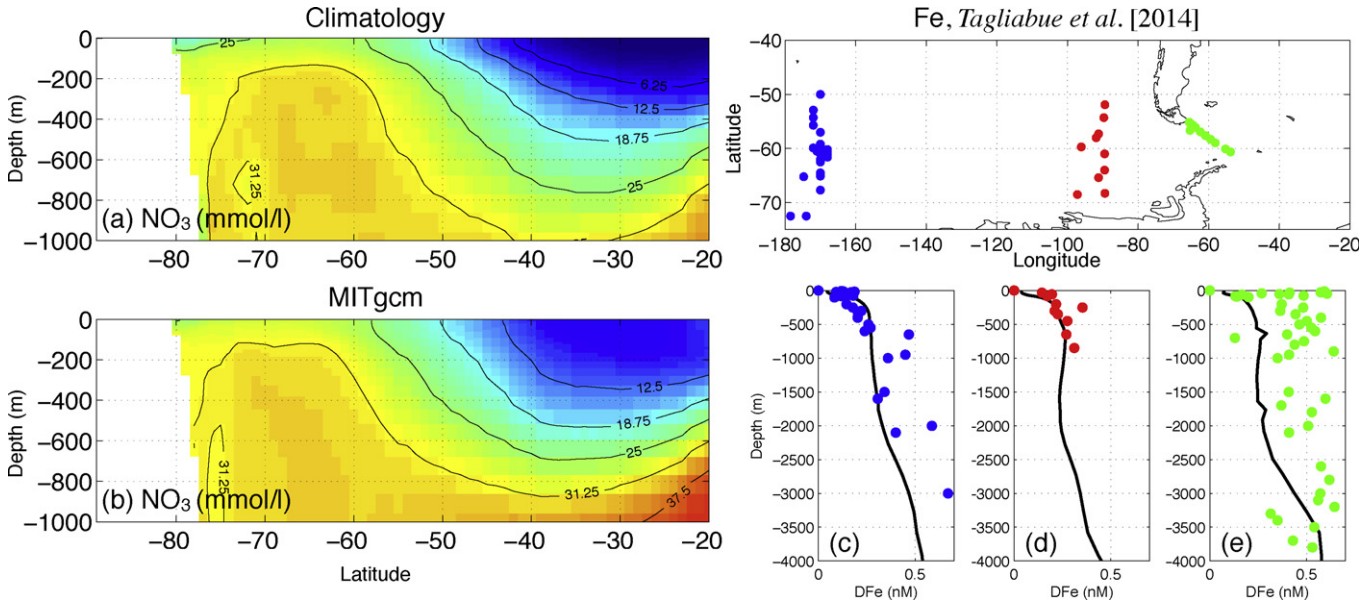

Fig. 1. Zonally averaged NO_3 (mmol/ł) in the Southern Ocean from the (a) climatology and (b) MITgcm. The simulated iron fields are compared with the observation along three meridional sections: near 170◦W (blue dots), near 90◦W (red dots) and the Drake Passage (green dots) as marked in the map. In (c–e), the solid lines represent the iron averaged over the sections in the model and the dots represent the iron observations from Tagliabue et al. (2014). (For interpretation of the references to color in this figure legend, the reader is referred to the web version of this article.)

the surface in both observations and model simulations. Fe concentrations increase with depth, and observations and model have similar vertical profiles of Fe when averaged meridionally (Fig. 1 (c, d)). Fe concentration across the Drake Passage is higher than the other two sections, particularly at the surface of the southern Drake Passage. Along the Drake Passage, the model underestimates Fe concentrations.

Although community productivity cannot be directly compared to chlorophyll concentration, the biological hot spot in the model coincides with areas of high chlorophyll biomass in satellite data

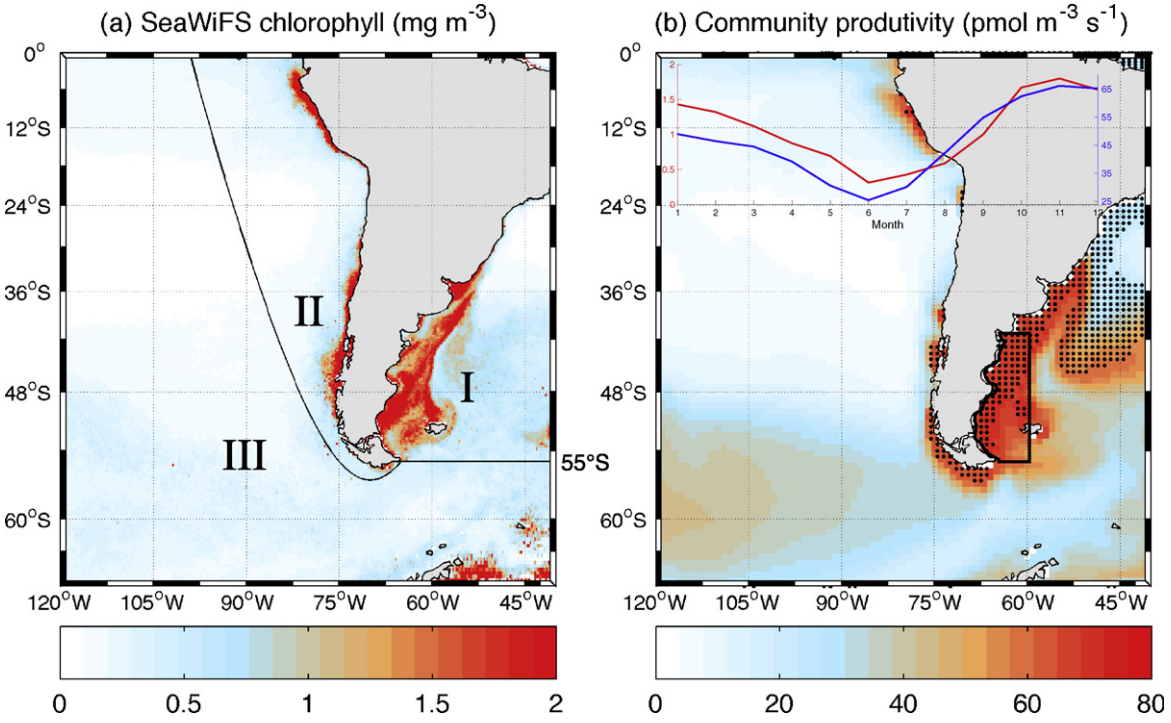

Fig. 2. (a) December chlorophyll averaged over 1997–2010 SeaWiFS data and (b) the December-mean simulated community productivity. The area marked with the black line in (b) is the area where the passive tracer is measured in the adjoint calculation. Time series of spatially-averaged chlorophyll (red) and community productivity (blue) in that area are inserted in (b). Three possible source regions are also marked as I, II and III in (a). The areas with black dots in (b) are where NO_3 is the limiting nutrient. (For interpretation of the references to color in this figure legend, the reader is referred to the web version of this article.)

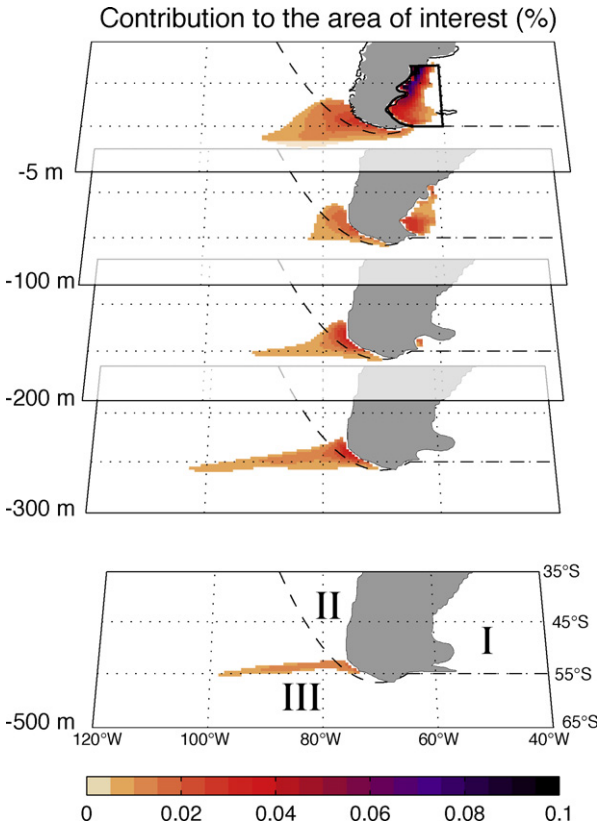

Fig. 3. The distribution of source waters one year prior to the arrival in the area of interest (marked with a black solid line) on the Patagonian shelf. The shading represents r_i, the relative contribution of each grid cell to the cost function change (see Eq. (B.2)). Grid cells with contributions less than 10^{-3}% are in white. Sums of all contributions from grid cells is 100%, although the maximum contribution is $O(10^{-1})$. Black dashed lines mark the boundaries between Regions I, II and III. (For interpretation of the references to color in this figure, the reader is referred to the web version of this article.)

(Fig. 2). Additionally, the seasonal cycle of community productivity is similar to that of chlorophyll biomass when averaged over the area shown in Fig. 2. In this simulation, the community productivity in the shelf regions in the southwestern Atlantic is mostly limited by NO_3 (the areas with black dots in Fig. 2 (b)), whereas community productivity is limited by Fe over most of the Southern Ocean.

3.2. Adjoint determination of source waters

Source waters that arrive over the Patagonian shelf after one year, as determined by the adjoint, are shown in Fig. 3. Broadly there are three supply regions: (I) waters local to the Patagonian shelf, (II) the southeast Pacific near the Chilean coast south of 42°S and (III) the southeast Pacific subsurface ocean along 55°S. They are labeled in Fig. 2 (a). In Region I, the depth of source waters is shallower than 200 m since here they are over the shelf. In Region II, the source waters are spread over the top 300 m, peaking near 250 m. Region III shows the deepest source, extending below 500 m. It is worth noting that regions south of 60°S do not "source" the Patagonian shelf, indicating that nutrient-rich water masses south of the Antarctic Circumpolar Current (ACC) are not involved in fueling productivity on the Patagonian shelf. Instead, nutrient-rich subsurface water to the north of the ACC is implicated.

Using adjoint sensitivity experiments, we can quantify the contribution of source waters to the area of interest (see Appendix B). The contributions of Regions I, II and III to the total passive tracer concentration at the Patagonian shelf, estimated following Eq.(B.1), are plotted in Fig. 4 (a). We also compute the relative contribution of NO_3 and Fe in the source waters after weighting by the adjoint sensitivity, and plot them in Fig. 4 (b, c), respectively. Region III is the largest contributor (Fig. 4 (a)), providing nearly half of the total passive tracer to the target area. Fig. 4 (b) shows that Region III is the largest pool of NO_3, contributing twice as much as Regions I and II. Region III contains the nutrient-rich deep water source (Fig. 1 (b)) and appears to be the largest supplier of NO_3 to the Patagonian shelf.

On the other hand, the largest Fe pool is Region I contributing almost half of the total Fe (Fig. 4 (c)). The geography of the Patagonian shelf enables Fe to be delivered to it rather readily from the sediment and atmosphere (both sources are simulated in the model; see Appendix A). Its wide shelf is an excellent source for Fe and there is substantial dust supply from Patagonia. The second largest Fe pool is Region III. In the Southern Ocean, Fe is depleted at the surface but increases with depth. Hence, the deep water source in Region III can also be a potent source of Fe.

3.3. Forward perturbation experiments

Perturbations in nutrients are introduced in one water source region at a time on June 1st, 7 months prior to the target date, at a concentration such that a 10% increase can be achieved at the Patagonian shelf if there is no consumption along the path, as described in Section 2.

Perturbations in NO_3 (δNO_3) have positive impacts on the NO_3 level (ΔNO_3) and the community productivity (ΔBIO) but negative impact on the Fe level (ΔFe) over the Patagonian shelf (Fig. 5 (a–c)). The δNO_3 in Region I triggers the immediate increase of NO_3 by approximately 10% because Region I encompasses the target area. The δNO_3 in Region I also has an immediate impact on the community productivity (Fig. 5 (c)). NO_3 is the limiting nutrient on the shelf, hence an additional NO_3 enhances the community productivity without delay. ΔNO_3 gradually decreases toward the end of the year as newly introduced NO_3 is continuously consumed (Fig. 5 (a)). As a result, ΔBIO also has a decreasing trend. The smallest ΔNO_3 in December by δNO_3 in Region I is associated with the largest response in the community productivity (2% increase in ΔBIO). This suggests that additional NO_3 in Region I is the most effective in promoting the community productivity on the shelf. The enhanced community productivity consumes Fe, resulting in a slight decrease in ΔFe in December.

δNO_3 in Regions II and III, in contrast, slowly increases the level of NO_3 and community productivity in the target area (Fig. 5 (a, c)). Regions II and III, upstream of Drake Passage, are distant from the Patagonian shelf and δNO_3 in those regions initially does not impact the biogeochemistry in the target area. As the water mass with additional NO_3 moves to the shelf, ΔNO_3 begins to grow and exceeds the 10% increase in December, suggesting that NO_3 is not heavily consumed before it is delivered to the Patagonian shelf. In December, the community productivity experiences a decreasing trend regardless of the perturbed region, suggesting that the consumption of NO_3 is faster than the supply of additional NO_3 on the shelf.

Perturbations in Fe (δFe) influence the Fe level (ΔFe) and the ΔBIO over the Patagonian shelf (Fig. 5 (d–f)). The ΔFe is increased by about 10% stemming from δFe in Region III, indicating that Fe is hardly consumed along its path (Fig. 5 (e)). In contrast, δFe in Region I is almost all consumed, resulting in only a slight increase (1.3%) after 7 months (Fig. 5 (e)). The δFe in Region I has almost no impact on the community productivity on the shelf even in June when additional Fe was introduced (Fig. 5 (f)). The largest ΔBIO over the shelf associated with Fe supply is caused by δFe in Region III, with Region II also contributing but to a lesser extent. Fe perturbations in Regions II and III elevate the community productivity in the Fe-limited area at the southeast

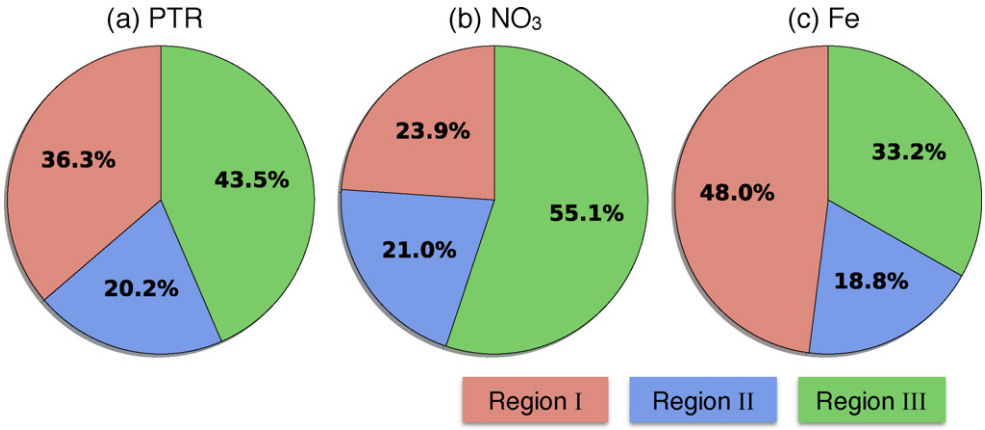

Fig. 4. (a) The relative passive tracer (PTR) contributions of Regions I (salmon), II (blue) and III (green) to the Patagonian shelf one year prior to arrival. The percentage of (b) NO_3 and (c) Fe at the source regions whose contribution is greater than 10^{-3}%is also computed after weighting these variables by adjoint sensitivity. (For interpretation of the references to color in this figure legend, the reader is referred to the web version of this article.)

corner of the target area. Fe perturbations in Region I remain on the northern shelf where Fe is not the limiting nutrient and lead to a very little impact on the community productivity (see Fig. 7).

Combined perturbations in both NO_3 and Fe (δNO_3 and δFe) result in changes in biogeochemistry on the shelf, and changes are similar to the sum of responses to δNO_3 and δFe separately (Fig. 5 (g–i)). ΔBIO is the largest with both δNO_3 and δFe (Fig. 5 (i)). This is to be expected because adding both nutrients relieves the nutrient limitation regardless of the type. Among water source regions, Region III has the most effect on the community productivity. Perturbations in Region I lead to the smallest increase in the community productivity 7 months later. This is because the additional Fe in Region I does not contribute to productivity but perturbations of both nutrients in Regions II and III can enhance productivity.

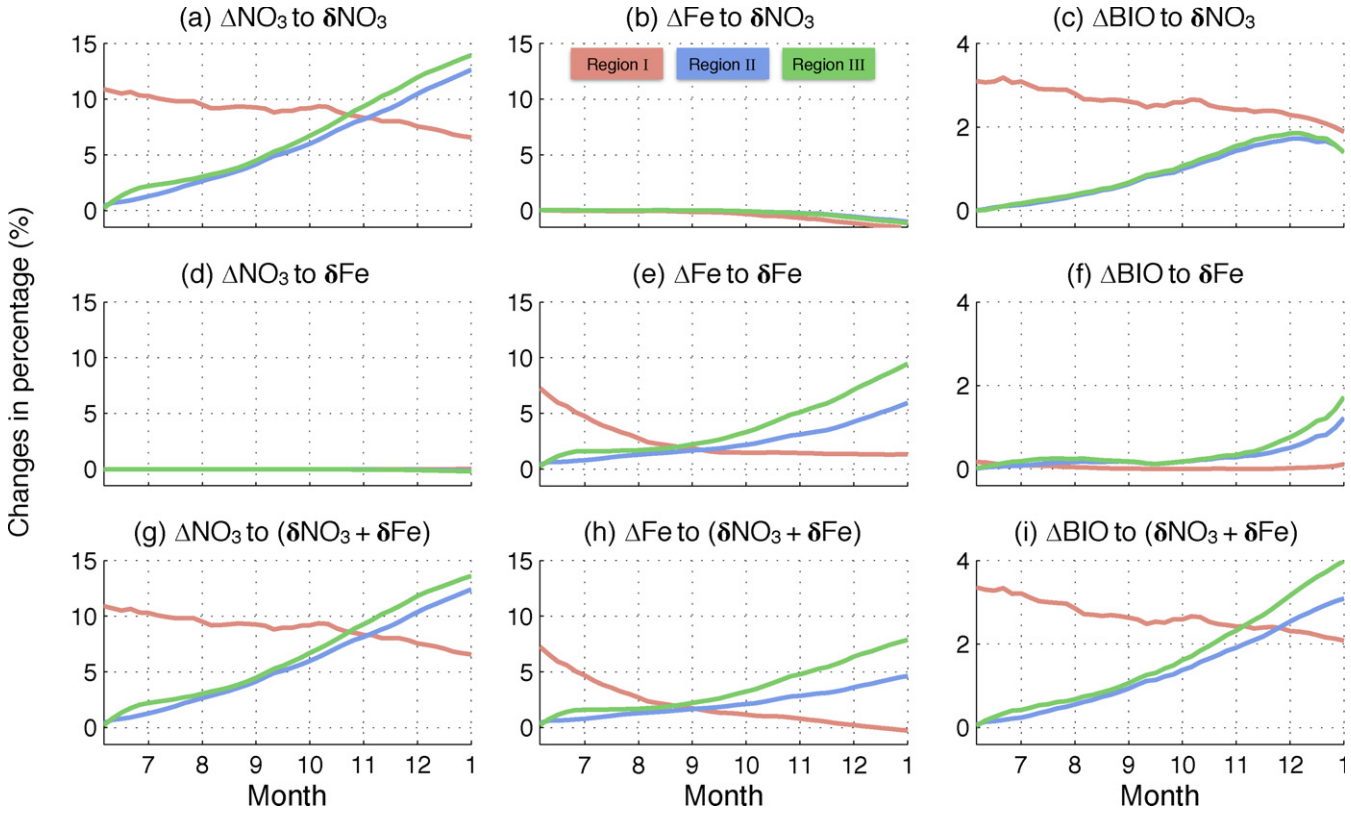

Fig. 5. Time series of the changes (%) in NO_3, Fe and community productivity (ΔNO_3, ΔFe and ΔBIO, respectively) at the target area to the perturbations of NO_3(δNO_3), Fe (δFe) and both nutrients introduced in Regions I (salmon), II (blue) and III (green) on June 1st. (For interpretation of the references to color in this figure legend, the reader is referred to the web version of this article.)

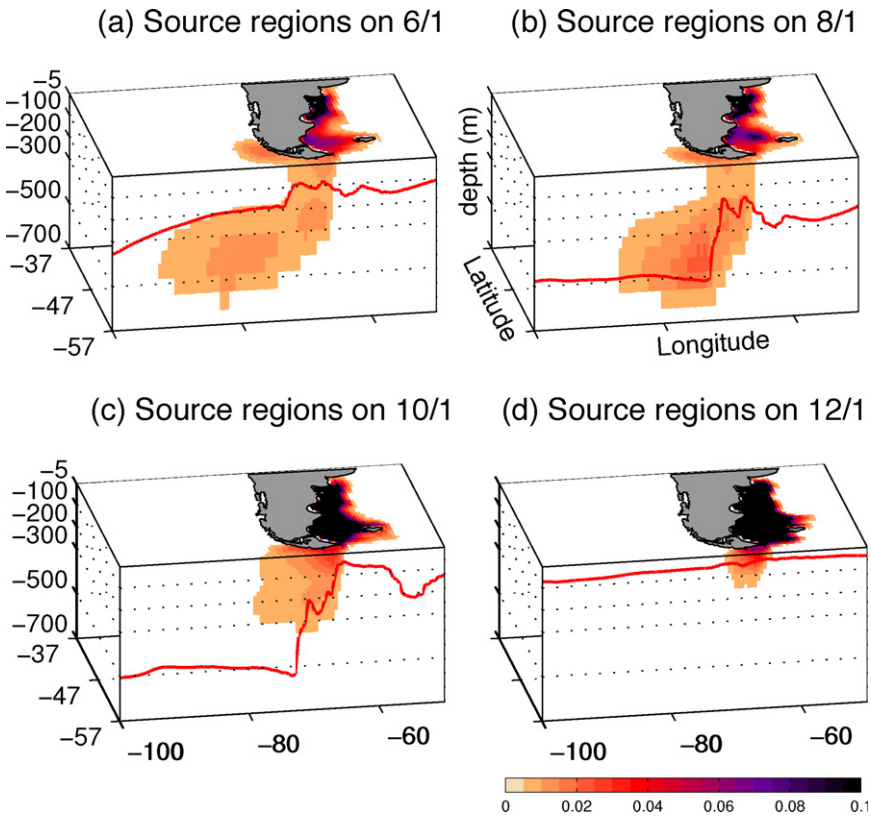

Fig. 6. Source waters (shaded) and mixed layer depth (red line) on (a) 6/1 or 7 months before, (b) 8/1 or 5 months before, (c) 10/1 or 3 months before and (d) 12/1 or 1 month before. The shading is the relative contribution as defined in Eq.(B.2). (For interpretation of the references to color in this figure legend, the reader is referred to the web version of this article.)

4. Discussion

4.1. How do source waters arrive at the Patagonian shelf?

The largest water source for the Patagonian shelf is Region III, the subsurface southeast Pacific ocean (Fig. 4 (a)). These waters arrive from a depth of 500 m or so along 55°S and are relatively rich in both NO_3 and Fe compared to other sources. They are a prime candidate to power new productivity on the Patagonian shelf. But how can water masses at depth (>300 m) be drawn to the surface within 7 months?

The Southern Ocean is characterized by persistent upwelling driven by strong westerly winds (Marshall and Speer, 2012). This upwelling is driven by a negative wind stress curl. However, given the value of this curl near the ACC ($O(10^{-7})$ N m^{-2}, Chelton et al. (2004)), the upwelling rates are only $O(10^{-1})$ m day^{-1}, too weak to bring the water at 300 m to the surface within a few months. Furthermore, source waters in Region III are in fact generally located north of the ACC where typically downwelling occurs. The vertical velocity related to the meridional overturning circulation can be estimated as $w = \partial\Psi/\partial y$, where Ψ is the stream function for the residual circulation: the estimated w is even smaller than the wind-driven circulation due to eddy compensation (Karsten and Marshall, 2002; Marshall et al., 2006).

Instead, a time series of adjoint sensitivity clearly shows that wintertime convective mixing is the main mechanism bringing deep waters to the surface (Fig. 6). On June 1st, source waters are below the mixed layer upstream of the Drake Passage. On August 1st, a sharp deepening of the mixed layer occurs resulting in the top 500 m of the water column becoming well mixed. The observed mixed-layer depth upstream of Drake Passage is found to be 500 m in winter (Dong et al., 2008; Forget et al., 2015b; Holte et al.,2012; Sallée et al., 2010). It is during this period that source waters can be drawn up to the surface. The mixed layer is still deep on October 1st when Region III waters begin to mix with those of Region II. The majority of the source waters arrive on the Patagonian shelf in December. The mixed layer shallows to less than 100 m in depth as the upper ocean is stratified in summer.

Wintertime vertical mixing in the Southern Ocean has been highlighted as a key to processes in Subantarctic Mode Water formation (McCartney, 1977; Talley, 1996), subduction of anthropogenic CO_2 (Sallée et al., 2012) and light limitation for phytoplankton growth (Cassar et al., 2011; Mitchell and Holm-Hansen, 1991; Sullivan et al., 1993). Wintertime intense vertical mixing is also thought to be responsible for Fe supply to the surface (Tagliabue et al., 2014). Our results show that community productivity on the shelf begins to respond in October (i.e. in the spring) to the Fe perturbation in Regions II and III (Fig. 5 (b)). This suggests that Fe becomes available to the shelf regions after wintertime intense vertical mixing upstream of Drake Passage.

4.2. Spatial patterns in the response of community productivity

The forward perturbation simulations guide us in understanding the biogeochemistry at work in the southwest Atlantic ocean. NO_3 perturbations result in an increase in community productivity on the Patagonian shelf where NO_3 is the limiting nutrient (Fig. 7 (a–c)). In particular, NO_3 perturbations in Region I lead to higher levels of community productivity over the northern part of the shelf (Fig. 7 (a)). In contrast, NO_3 perturbations in Regions II and III enhance community productivity on the southern margin of the shelf. Additionally, enhanced NO_3 input in Regions II and III shrinks the NO_3-limited region over the southern part of the shelf (Fig. 7 (b, c)).

The additional Fe introduced in Region I has almost no effect on community productivity over the Patagonian shelf where Fe is not

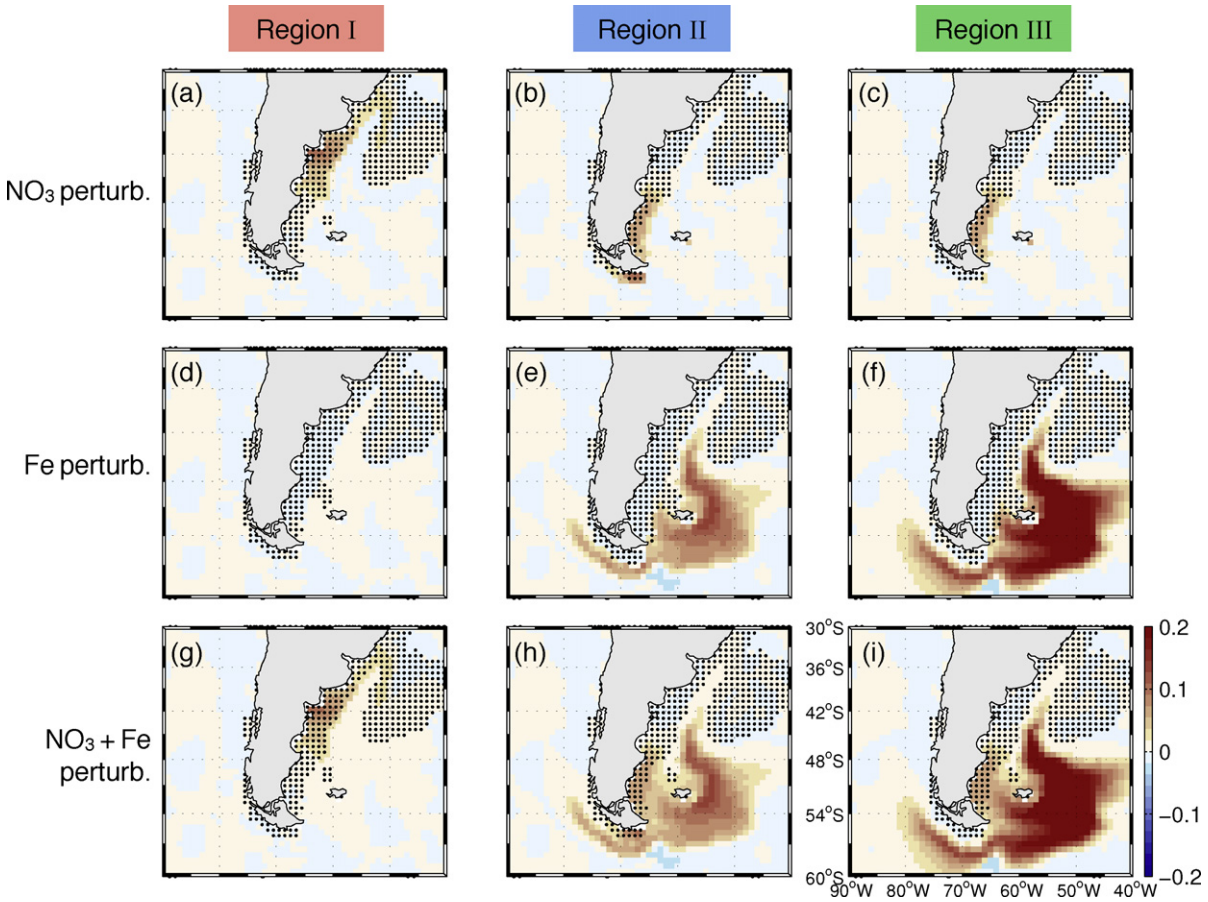

Fig. 7. Changes of the community productivity to the perturbations in (a–c) NO_3, (d–f) Fe and (g–i) both nutrients (0.1 = 10%). Perturbations are introduced in Regions (a, d, g) I, (b, e, h) II and (c, f, i) III on June 1st, or 7 months prior to the time when the responses are calculated. Black dots represent the region with NO_3 limitation.

the limiting nutrient (Fig. 7 (d)). When more Fe is added in regions with nonzero adjoint sensitivity on the shelf (colored area in Fig. 3), the community productivity offshore of the shelf break does not change, indicating that the source waters over the shelf are trapped there. Fe perturbations in Regions II and III also do not increase community productivity in the NO_3-limited shelf region. Instead, they promote community productivity offshore (Fig. 7 (e, f)). Although the increase of community productivity due to Fe is smaller than that due to NO_3 over the shelf (Fig. 5 (c, f)), the Fe perturbations lead to a larger increase of community productivity integrated over the southwest Atlantic. The additional Fe from Region III boosts community productivity by up to 30%. The size of the NO_3-limited area extends over most of the Patagonian shelf as more Fe is introduced there.

The combined increase of NO_3 and Fe in Region I increases community productivity but only over the northern part of the shelf (Fig. 7 (g)), similar to the NO_3 perturbation case. The extra NO_3 and Fe from Regions II and III enhance productivity over both the shelf and offshore of the shelf break. The enhanced community productivity upstream of Drake Passage indicates where nutrient-rich water is upwelled. The addition of NO_3 and Fe in Region III leads to the greatest enhancement of community productivity in the southwest Atlantic ocean (Fig. 7 (i)).

4.3. Increasing trend of chlorophyll biomass

Rivas et al. (2006) report an increasing trend of the chlorophyll maximum observed from SeaWiFS data during 1998 to 2003 over the Patagonian shelf. They argue that higher nutrient supply together with a more stratified water column is a main driver of the trend. Other studies consistently show an increasing chlorophyll trend offshore of the Patagonian shelf (Gregg et al., 2005; Gregg and Rousseaux, 2014; Henson et al., 2010; Siegel et al., 2013; Vantrepotte and Mèlin, 2011). This increasing trend has been explained in terms of temperature trends (Gregg et al., 2005; Siegel et al., 2013) and trends in the Southern Annular Mode (SAM) (Vantrepotte and Mèlin, 2011).

Our study suggests that nutrient supply to the southwest Atlantic relies on wintertime vertical mixing. If there is a long-term deeper wintertime mixed layer, it is likely that the southwest Atlantic will be more replete with nutrients. Sallée et al. (2010) show that mixed layer depths are largely modulated by SAM, and there has been a deepening mixed layer trend upstream of Drake Passage. The deepening of the mixed layer potentially brings more nutrient to the surface which can be subsequently transported to the Patagonian shelf by the ACC. Based upon our findings, community productivity and chlorophyll biomass will also show an increasing trend.

5. Conclusion

We have explored how the ocean supplies nutrients to the Patagonian shelf, one of the most productive areas in the global ocean with intense CO_2 uptake. Three regions were identified as significant sources: (I) the Patagonian shelf itself, (II) the southeast Pacific near the Chilean coast and (III) the subsurface ocean upstream along

Table 1
Parameter names, values and units for the biogeochemical model.

Parameter name	Value	Units
Light		
Light attenuation coefficient	0.014	m^{-1}
Self-shading coefficient	0.07	$m^2\ mg^{-1}$
Photosynthetically active radiation	0.4	Nondimensional
Half saturation light constant (K_I)	30	$W\ m^{-2}$
Community productivity		
Maximum consumption rate (α)	0.33	$\mu M\ month^{-1}$
Half saturation NO_3 constant (K_{NO_3})	8	μM
Half saturation Fe constant (K_{Fe})	0.1	nM
Fraction of new production to DON pool	0.67	Nondimensional
Time scale for DON remineralization	6	month
N:Fe stoichiometry	0.016	Nondimensional
Iron		
Scavenging rate	0.2×10^{-7}	s^{-1}
Ratio of sediment Fe to NO_3 flux (β)	1.153	Nondimensional
Minimum Fe flux from sediment ($F_{Fe,0}$)	0.001	$pM\ s^{-1}$

the ACC in the Southeast Pacific. Region III was found to be most responsible for providing tracers to the Patagonian shelf.

The northern part of the shelf receives waters from regions local to the shelf. This water mass is rich in Fe but remains on the shelf where macronutrient is limited. Hence, in our calculations, only additional NO_3 can enhance the community productivity over the shelf. The source waters for the southern shelf and offshore are found at depth in the southeast Pacific in Region III. In our biogeochemical model, NO_3 perturbations applied in that source region result in higher community productivity over the shelf where NO_3 is the limiting factor. Fe perturbations, on the other hand, lead to an increase of community productivity offshore where Fe is the limiting factor. Our study further shows that intense wintertime vertical mixing is the key process drawing high nutrients from the subsurface of the southeast Pacific to the surface and preconditioning nutrient fields to spur biological productivity in the following spring in the southwest Atlantic.

Acknowledgments

We gratefully acknowledge NSF support of the MOBY project (grant OCE-1048926). The authors would like to thank two anonymous reviewers for valuable comments and suggestions, which significantly improved the manuscript.

Appendix A. Biogeochemical model

The biogeochemical model includes the cycling of carbon, NO_3 and Fe through abiotic and biotic processes in the ocean column following Parekh et al. (2005) and Dutkiewicz et al. (2006). The model does not include an explicit ecosystem but instead parameterizes the export of organic matter from the surface ocean. The biological uptake of inorganic nutrients is parameterized as a function of light and nutrients:

$$B = \alpha \frac{I}{I + K_I} min\left(\frac{NO_3}{NO_3 + K_{NO_3}}, \frac{Fe}{Fe + K_{Fe}}\right), \tag{A.1}$$

where α is maximum uptake rate, K_I, K_{NO_3} and K_{Fe} are the half saturation constants for the light, NO_3 and Fe, respectively. A fraction of B enters a dissolved organic pool which remineralizes with a timescale of 6 months. The remaining fraction of B is instantaneously exported to depth and remineralized following a power law relationship (Martin et al., 1987). B can thus be likened to "community production" as it includes the impact of herbivores as well as primary produces. It cannot therefore be directly compared to "primary production" or chlorophyll. However, it should have similar patterns to metrics of productivity in the surface ocean. By not representing the timescales of the organic matter to pass through living phases, the timing of some surface biological processes will not be captured. However here the focus is on deep nutrient sources which will be adequately captured.

The model includes both aeolian and sediment sources of Fe. The latter is an improvement over the older studies such as Dutkiewicz et al. (2006), Ito et al. (2005), Parekh et al. (2005) that used this same biogeochemical model. The Fe dust data is extracted from the preindustrial value in Luo et al. (2008). The sediment Fe source is added following Elrod et al. (2004) where the flux of Fe is expressed as a function of a flux of organic matter to sediment based on the observations in California. The parameter choices (see Table 1) are similar to those used in our previous models, though specific parameters were tuned to yield spatial and temporal variability of B similar to that for chlorophyll. In particular, the parameter α includes many aspects of the ecosystem not otherwise captured, such as grazing, and limitation by other nutrients. See Parekh et al. (2004,2006) and Dutkiewicz et al. (2005) for full equations. This simple biogeochemical model is significantly faster than one including a full ecosystem allowing long spin-up to quasi-equilibrium. Yet, this model also provides nutrient fields and productivity that compare well to observations (see Fig. 1 as well as results from our previous studies, Dutkiewicz et al. 2006; Ito et al. 2005; Parekh et al. 2005; Verdy et al. 2007).

Appendix B. Adjoint model setting

The contribution of source waters to the area of interest can be quantified using the adjoint sensitivity. The change in J, δJ, due to a perturbation $\delta x = [\delta x_1, \delta x_2, \cdots, \delta x_N]$ to the state $x = [x_1, x_2, \cdots, x_N]$ at an earlier time can be written as

$$\delta J = \frac{\partial J}{\partial x_1}\delta x_1 + \frac{\partial J}{\partial x_2}\delta x_2 + \cdots + \frac{\partial J}{\partial x_n}\delta x_N. \tag{B.1}$$

When $\delta x_1 = \delta x_2 = \cdots = \delta x_N = 1$ in Eq.(B.1), δJ is the sum of all the sensitivities, $\Sigma_{i=1}^{N} \partial J/\partial x_i$. Hence the relative contribution of x_i to δJ, r_i, is simply the ratio between $\partial J/\partial x_i$ and $\Sigma_{i=1}^{N} \partial J/\partial x_i$, or expressed as a percentage,

$$r_i = \frac{\partial J/\partial x_i}{\Sigma_{i=1}^{N} \partial J/\partial x_i} \times 100. \tag{B.2}$$

References

M.F., Acha, E.M., Mianzan, H.W., Guerrero, R.A., Bava, J., 2004. Marine fronts at the continental shelves of austral South America: physical and ecological processes. J. Mar. Syst. 44 (1-2), 83–105.

Adcroft, A., Hill, C., Marshall, J., 1997. Representation of topography by shaved cells in a height coordinate ocean model. Mon. Weather Rev. 125, 2293–2315.

Adcroft, A.C.H., Marshall, J., 1999. A new treatment of the coriolis terms in c-grid models at both high and low resolutions. Mon. Weather Rev. 127, 1928–1936.

A.P., Bianchi, A.A., Bianucci, L., Piola, A.R., Pino, D.R., Schloss, I., Balestrini, C.F., 2005. Vertical stratification and air–sea CO_2 fluxes in the Patagonian shelf. J. Geophys. Res. 110, C07003

Bianchi, A.A., Pino, D.R., Perlender, H.G.I., Osiroff, A.P., Segura, V., Lutz, V., Clara, M.L., Balestrini, C.F., Piola, A.R., 2009. Annual balance and seasonal variability of sea–air CO_2 fluxes in the Patagonia Sea: their relationship with fronts and chlorophyll distribution. J. Geophys. Res. 114, C03018

Bisbal, G.A., 1995. The Southeast South American shelf large marine ecosystem: evolution and components. Mar. Policy 19 (1), 21–38.

Cassar, N., Difiore, P., Barnett, B., Bender, M., Bowie, A., Tilbrook, B., Petrou, K., Westwood, K., Wright, S., Lefevre, D., 2011. The influence of iron and light on net community production in the Subantarctic and Polar Frontal Zones. Biogeosciences 8, 227–237.

Chelton, D.B., Schlax, M.G., Freilich, M.H., Milliff, R.F., 2004. Satellite measurements reveal persistent small-scale features in ocean winds. Science 303 (5660), 978–983.

Chhak, K., Di Lorenzo, E., 2007. Decadal variations in the California Current upwelling cells. Geophys. Res. Lett. 34 (14),
Dong, S., Sprintall, J., Gille, S.T., Talley, L., 2008. Southern Ocean mixed-layer depth from Argo float profiles. J. Geophys. Res. 113, C06013
Dutkiewicz, S., Follows, M.J., Heimbach, P., Marshall, J., 2006. Controls on ocean productivity and air–sea carbon flux: an adjoint model sensitivity study. Geophys. Res. Lett. 33, L02603
Dutkiewicz, S., Sokolov, A., Scott, J., Stone, P., 2005. A three-dimensional ocean-seaice–carbon cycle model and its coupling to a two-dimensional atmospheric model: uses in climate change studies. Joint Program on the Sci. Policy Global Change. MIT, Cambridge, Mass. Ch. Rep. 122.
Elrod, V.A., Berelson, W.M., Coale, K.H., Johnson, K.S., 2004. The flux of iron from continental shelf sediments: a missing source for global budgets. Geophys. Res. Lett. 31, L12307
Forget, G., Campin, J.M., Heimbach, P., Hill, C.N., Ponte, R.M., Wunsch, C., 2015. ECCO version 4: an integrated framework for non-linear inverse modeling and global ocean state estimation. Geosci. Model Dev. 8 (5), 3653–3743.
Forget, G., Ferreira, D., Liang, X., 2015. On the observability of turbulent transport rates by Argo: supporting evidence from an inversion experiment. Ocean Sci. 12 (3), 1107–1143.
Fukumori, I., Lee, T., Cheng, B., Menemenlis, D., 2004. The origin, pathway, and destination of ni no-3 water estimated by a simulated passive tracer and its adjoint. J. Phys. Oceanogr. 34 (3), 582–604.
Fukumori, I., Wang, O., Llovel, W., Fenty, I., Forget, G., 2015. A near-uniform fluctuation of ocean bottom pressure and sea level across the deep ocean basins of the Arctic Ocean and the Nordic Seas. Prog. Oceanogr. 134, 152–172.
Garcia, V.M., Garcia, C.A., Mata, M.M., Pollery, R.C., Piola, A.R., Signorini, S.R., McClain, C.R., Iglesias-Rodriguez, M.D., 2008. Environmental factors controlling the phytoplankton blooms at the Patagonia shelf-break in spring. Deep-sea Res. I 55 (9), 1150–1166.
Gent, P.R., McWilliams, J.C., 1990. Isopycnal mixing in ocean circulation models. J. Phys. Oceanogr. 20, 150–155.
Gregg, W.W., Casey, N.W., McClain, C.R., 2005. Recent trends in global ocean chlorophyll. Geophys. Res. Lett. 32, L03606
Gregg, W.W., Rousseaux, C.S., 2014. Decadal trends in global pelagic ocean chlorophyll: a new assessment integrating multiple satellites, in situ data, and models. J. Geophys. Res. Oceans 119, 5921–5933.
Henson, S.A., Sarmiento, J.L., Dunne, J.P., Bopp, L., Lima, I., Doney, S.C., John, J., Beaulieu, C., 2010. Detection of anthropogenic climate change in satellite records of ocean chlorophyll and productivity. Biogeosciences 7, 621–640.
Hill, C.N., Bugion, V., Follows, M.J., Marshall, J.C., 2004. Evaluating carbon sequestration efficiency in an ocean model using adjoint sensitivity analysis. J. Geophys. Res. 109, C11005
Holte, J.W., Talley, L.D., Chereskin, T.K., Sloyan, B.M., 2012. The role of air–sea fluxes in Subantarctic Mode Water formation. J. Geophys. Res. 117, C03040
Ito, T., Parekh, P., Dutkiewicz, S., Follows, M., 2005. The antarctic circumpolar productivity belt. Geophys. Res. Lett. 32, L13604
Karsten, R.H., Marshall, J., 2002. Constructing the residual circulation of the ACC from observations. J. Phys. Oceanogr. 32, 3315–3327.
Luo, C., Mahowald, N., Bond, T., Chuang, P.Y., Artaxo, P., Siefert, R., Chen, Y., Schauer, J., 2008. Combustion iron distribution and deposition. Glob. Biogeochem. Cycles 22, GB1012
Machado, I., Barreiro, M., Calliari, D., 2013. Variability of chlorophyll-a in the southwestern atlantic from satellite images: seasonal cycle and enso influences. Cont. Shelf Res. 53, 102–109.
Marotzke, J., Giering, R., Zhang, K.Q., Stammer, D., Hill, C., Lee, T., 1999. Construction of the adjoint MIT ocean general circulation model and application to Atlantic heat transport sensitivity. J. Geophys. Res. 104 (C12), 29529–29547.
Marshall, J., Adcroft, A., Hill, C., Perelman, L., Heisey, C., 1997. A finite-volume, incompressible Navier Stokes model for studies of the ocean on parallel computers. J. Geophys. Res. 102 (C3), 5753–5766.
Marshall, J., Hill, C., Perelman, L., Adcroft, A., 1997. Hydrostatic, quasi-hydrostatic, and nonhydrostatic ocean modeling. J. Geophys. Res. 102 (C3), 5733–5752.
Marshall, J., Jones, H., Hill, C., 1998. Efficient ocean modeling using non-hydrostatic algorithms. J. Mar. Syst. 18, 115–134.
Marshall, J., Shuckburgh, E., Jones, H., Hill, C., 2006. Estimates and implications of surface eddy diffusivity in the Southern Ocean derived from tracer transport. J. Phys. Oceanogr. 36, 1806–1821.
Marshall, J., Speer, K., 2012. Closure of the meridional overturning circulation through Southern Ocean upwelling. Nat. Geosci. 5, 171–180.
Martin, J.H., Knauer, G.A., Karl, D.M., Broenkow, W.W., 1987. VERTEX: carbon cycling in the northeast Pacific. Deep Sea Res. A 34 (2A), 267–285.
McCartney, M.S., 1977. Subantarctic mode water. In: Angel, M. (Ed.), A Voyage of Discovery: George Deacon 70Th Anniversary Volume. Pergamon Press, Oxford, pp. 103–119.
Mitchell, B.G., Holm-Hansen, O., 1991. Observations of modeling of the Antartic phytoplankton crop in relation to mixing depth. Deep-sea Res. Pt. A 38 (8), 981–1007.
Moore, A.M., Arango, H.G., Di Lorenzo, E., Miller, A.J., Cornuelle, B.D., 2009. An adjoint sensitivity analysis of the Southern California Current circulation and ecosystem. J. Phys. Oceanogr. 39 (3), 702–720.
Padín, X.A., Vázquez Rodríguez, M., Castano, M., Velo, A., Alonso Pérez, F., Gago, J., Gilcoto, M., Álvarez, M., Pardo, P.C., de la Paz, M., Ríos, A.F., Pérez, F.F., 2010. Air–sea CO_2 fluxes in the Atlantic as measured during boreal spring and autumn. Biogeosciences 7 (5), 1587–1606.
Palma, E.D., Matano, R.P., Piola, A.R., 2008. A numerical study of the Southwestern Atlantic Shelf circulation: stratified ocean response to local and offshore forcing. J. Geophys. Res. 113, C11010
Paparazzo, F.E., Bianucci, L., Schloss, I.R., Almandoz, G.O., Solís, M., Esteves, J.L., 2010. Cross-frontal distribution of inorganic nutrients and chlorophyll-a on the Patagonian continental shelf of argentina during summer and fall. Rev. Biol. Mar. Oceanogr. 45 (1), 107–119.
Parekh, P., Follows, M., Boyle, E., 2004. Modeling the global ocean iron cycle. Glob. Biogeochem. Cycles 18, GB1002
Parekh, P., Follows, M.J., Boyle, E.A., 2005. Decoupling of iron and phosphate in the global ocean. Glob. Biogeochem. Cycles 19, GB2020
Parekh, P., Follows, M.J., Dutkiewicz, S., Ito, T., 2006. Physical and biological regulation of the soft tissue carbon pump. Paleoceanography 21, PA3001
Redi, M.H., 1982. Oceanic isopycnal mixing by coordinate rotation. J. Phys. Oceanogr. 12, 1154–1158.
Rivas, A.L., Dogliotti, A.I., Gagliardini, D.A., 2006. Seasonal variability in satellite-measured surface chlorophyll in the Patagonian Shelf. Cont. Shelf Res. 26 (6), 703–720.
Romero, S.I., Piola, A.R., Charo, M., Garcia, C.A.E., 2006. Chlorophyll-a variability off Patagonia based on seawiFS data. J. Geophys. Res. 111, C05021
Sabatini, M., Reta, R., Matano, R., 2004. Circulation and zooplankton biomass distribution over the southern Patagonian shelf during late summer. Cont. Shelf Res. 24 (12), 1359–1373.
Sallée, J.B., Matear, R.J., Rintoul, S.R., Lenton, A., 2012. Localized subduction of anthropogenic carbon dioxide in the southern hemisphere oceans. Nat. Geosci. 5 (8), 579–584.
Sallée, J.B., Speer, K., Rintoul, S., 2010. Zonally asymmetric response of the Southern Ocean mixed-layer depth to the Southern Annular Mode. Nat. Geosci. 3, 273–279.
Siegel, D., Behrenfeld, M., Maritorena, S., McClain, C., Antoine, D., Bailey, S., Bontempi, P., Boss, E., Dierssen, H., Doney, S., Jr, R.E., Evans, R., Feldman, G., Fields, E., Franz, B., Kuring, N., Mengelt, C., Nelson, N., Patt, F., Robinson, W., Sarmiento, J., Swan, C., Werdell, P., Westberry, T., Wilding, J., Yoder, J., 2013. Regional to global assessments of phytoplankton dynamics from the seawiFS mission. Remote Sens. Environ. 135 (0), 77–91.
Song, H., Miller, A.J., Cornuelle, B.D., Di Lorenzo, E., 2011. Changes in upwelling and its water sources in the California Current system driven by different wind forcing. Dyn. Atmos. Oceans 52 (1), 170–191.
Song, H., Miller, A.J., McClatchie, S., Weber, E.D., Nieto, K.M., Checkley, D.M., 2012. Application of a data-assimilation model to variability of Pacific sardine spawning and survivor habitats with ENSO in the California Current System. J. Geophys. Res. Oceans 117, C03009
Sullivan, C., Arrigo, K., McClain, C., Comiso, J., Firestone, J., 1993. Distributions of phytoplankton blooms in the Southern Ocean. Science 262 (5141), 1832–1837.
Tagliabue, A., Sallée, J.B., Bowie, A.R., Lévy, M., Swart, S., Boyd, P.W., 2014. Surface-water iron supplies in the Southern Ocean sustained by deep winter mixing. Nat. Geosci. 7, 314–320.
Takahashi, T., Sutherland, S., Sweeney, C., Poisson, A., Metzl, N., Tillbrook, B., Bates, N., Wanninkhof, R., Feely, R., Sabine, C., Olafsson, J., Nojiri, Y., 2002. Global seaair CO_2 flux based on climatological surface ocean pCO_2, and seasonal biological and temperature effects. Deep-Sea Res. II 49, 1601–1622.
Talley, L.D., 1996. Antarctic intermediate water in the south atlantic. In: G.W., et al (Ed.), The South Atlantic: Present and Past Circulation. Springer, Berlin, pp. 219–238.
Vantrepotte, V., Mèlin, F., 2011. Inter-annual variations in the seawiFS global chlorophyll a concentration (1997–2007). Deep-Sea Res. I 58, 429–441.
Verdy, A., Dutkiewicz, S., Follows, M.J., Marshall, J., Czaja, A., 2007. Carbon dioxide and oxygen fluxes in the southern ocean: mechanisms of interannual variability. Glob. Biogeochem. Cycles 21, GB2020.